Geometry optimization for dark soliton combs in thin multimode silicon nitride microresonators

YAOJING ZHANG,[1,†] **SHUANGYOU ZHANG,**[1,3,†] **TOBY BI,**[1,2] **AND PASCAL DEL'HAYE**[1,2,4]

[1]*Max Planck Institute for the Science of Light, 91058 Erlangen, Germany*
[2]*Department of Physics, Friedrich-Alexander-Universität Erlangen-Nürnberg, 91058 Erlangen, Germany*
[3]*shuangyou.zhang@mpl.mpg.de*
[4]*pascal.delhaye@mpl.mpg.de*
[†]These authors contributed equally

Abstract: Silicon nitride (Si_3N_4) has been well established as an ultralow-loss material for integrated photonics, particularly for the generation of dissipative Kerr soliton frequency combs, enabling various applications for optical metrology, biological imaging, and coherent telecommunications. Typically, bright soliton generation in Si_3N_4 devices requires thick (>600 nm) films to fulfill the condition of anomalous dispersion at telecom wavelengths. However, thick films of ultralow-loss Si_3N_4 (>400 nm) often suffer from high internal stress, leading to cracks. As an alternative approach, thin Si_3N_4 films (<400 nm) provide the advantage of one-step deposition and are widely applied for commercial use. Here, we provide insights into engineering an integrated Si_3N_4 structure that achieves optimal effective nonlinearity and maintains a compact footprint. A comparative analysis of Si_3N_4 resonators with varying waveguide thicknesses is conducted and reveals that a 400-nm thin Si_3N_4 film emerges as a promising solution that strikes a balance among the aforementioned criteria. Based on a commercially available 400-nm Si_3N_4 film, we experimentally demonstrate the generation of low-noise coherent dark pulses with a repetition rate of 25 GHz in a multimode Si_3N_4 resonator. The compact spiral-shaped resonator has a footprint of 0.28 mm^2 with a high-quality factor of 4×10^6. Our demonstrated dark combs with mode spacings of tens of GHz have applications in microwave photonics, optical spectroscopy, and telecommunication systems.

1. Introduction

Integrated photonic circuits based on silicon nitride (Si_3N_4) are extensively used for microresonator based optical frequency comb generation. Si_3N_4 provides compatibility with complementary metal–oxide–semiconductor (CMOS) fabrication processes and has a large bandgap covering a wide spectral transparency window [1], without suffering from nonlinear absorption, which is problematic in silicon photonic circuits [2,3]. In addition, Si_3N_4 exhibits a relatively high Kerr nonlinearity compared to silica. Thus, many applications have been demonstrated with Si_3N_4 based microresonators, including optical spectroscopy [4], biological imaging [5,6], and telecommunications [7,8]. Recent developments include heterogeneously integrated laser soliton microcombs on a monolithic silicon substrate via integrating semiconductor lasers with Si_3N_4 microresonators [9]. Using III-V-on-silicon photonic integration, a chip-scale photonic system has been successfully used for optical data transmission and microwave photonics [10]. There has been growing interest in the integration of frequency combs for optical computing and optical neural networks, as well as for parallel convolutional and photonic convolutional accelerators [11].

The generation of soliton microcombs in Si_3N_4 microresonators relies on achieving both ultrahigh quality (Q) factors (low losses) and well-defined waveguide dimensions to engineer the dispersion properties of the microresonators. This is of particular importance because resonator

dispersion plays a critical role in determining the temporal dynamics of soliton microcombs. Typically, bright soliton microcombs are generated by pumping in the anomalous dispersion regime [12–14] while mode-locked dark pulses in microresonators require normal dispersion [15,16]. Dark-bright soliton pairs can be generated across these two distinct dispersion regimes [17]. Recently, zero-dispersion solitons have also attracted intensive research interest [18–21]. For Si_3N_4 resonators, anomalous dispersion usually requires film thicknesses >600 nm in the telecom band. Low-pressure chemical vapor deposition (LPCVD) is a commonly used method for fabricating such Si_3N_4 films with low propagation loss. However, the required high deposition temperature (~800 °C) typically results in high stress, leading to the formation of fatal cracks that limit the film thickness to 400 nm. Consequently, the production of thick Si_3N_4 films (>400 nm) requires more complex processes, including patterning crack barriers in the underlying SiO_2 layer, multi-step deposition, multiple annealing cycles, or the photonic Damascene process [22]. More recently, it has been shown that thicker Si_3N_4 films with low stress can be obtained by combining a thin layer of LPCVD nitride with a second layer from plasma-enhanced chemical vapor deposition (PECVD) [23].

In contrast, thin Si_3N_4 films (<400 nm) can be fabricated through a simpler one-step deposition process [24]. It is worth noting that Si_3N_4 films with thicknesses of 400 nm are readily available as commercial products. Although these films typically exhibit normal dispersion, their advantages of uncomplicated deposition and widespread industrial availability make them highly appealing for generating dark soliton microcombs. The generation of dark combs in the normal dispersion regime is often facilitated by mode interactions between different mode families [25]. This has been demonstrated in 550-nm [15,26,27] and 600-nm [28–32] thick Si_3N_4 microresonators, in which multimode waveguides were used to realize different spatial mode families. In recent developments, the generation of dark combs has been achieved through the technique of self-injection locking, eliminating the need for mode crossings [33]. Ultra-thin Si_3N_4 (< 100 nm) resonators exhibit remarkably high Q factors surpassing 10^8, however, at the cost of larger mode volumes since a large fraction of the light is within the cladding material. Applications for these resonators extend to both linear and nonlinear applications, including linewidth narrowing of diode lasers [33], and on-chip turnkey soliton microcombs [34]. The low confinement of the modes requires quite large resonators in these structures in order to avoid losses. In addition, these structures need very thick (> 10 μm) high-quality SiO_2 layers.

In this study, we thoroughly investigate the optical properties of Si_3N_4 resonators across different waveguide thicknesses. In particular, we investigate the ideal waveguide dimensions that provide good confinement as well as high effective nonlinearities. Here we find that a Si_3N_4 thickness of around 400 nm provides a sweet spot for good confinement as well as good effective nonlinearity in the telecom band. By using commercially available 400-nm Si_3N_4 films, we experimentally demonstrate low-noise dark combs in a high-Q (4×10^6) Si_3N_4 multimode microresonator. The resonator has a compact footprint of 0.28 mm^2 with a spiral shape. The dark combs have mode spacings of 25 GHz.
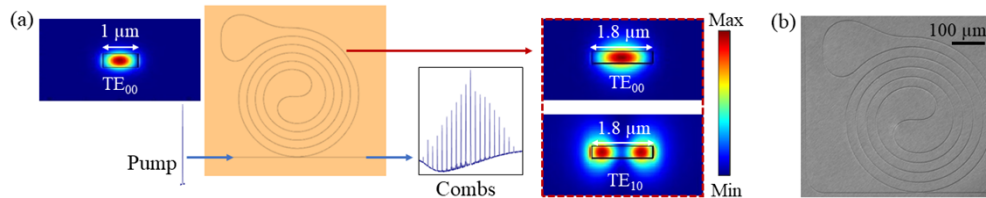
2. Design of compact multimode Si_3N_4 resonators

Figure 1(a) shows a schematic of the Si_3N_4 chip. It consists of a core Si_3N_4 layer, a cladding layer (silica), and a bottom layer (silica), which are all on top of a silicon substrate. We first calculate the effective nonlinear refractive index $n_{2,\text{eff}}$ and confinement factor Γ of a Si_3N_4 waveguide as a function of Si_3N_4 thickness in the range between 60 nm to 1000 nm as shown in Fig. 1(b) and Fig. 1(c). Here, $n_{2,\text{eff}}$ is the average nonlinear refractive index taking into account that the mode is partially in Si_3N_4 and partially in the silica cladding [35]. The thicknesses of the silica top and bottom layers are set to 3 μm. For comparison, the $n_{2,\text{eff}}$ is calculated at three distinct waveguide widths of 1 μm, 1.8 μm, and 3 μm. Based on our simulation results, the three curves exhibit an initial increase as the thickness of Si_3N_4 rises, subsequently peaking around a thickness range

of 400-450 nm. However, a further increase in the thickness of the Si_3N_4 film would lead to a decrease in the value of $n_{2,\mathrm{eff}}$. The $n_{2,\mathrm{eff}}$ reaches its maximum with a waveguide width of 3 μm and thickness of 420 nm. The confinement factor Γ is defined as the ratio of the time-averaged energy flow through the core waveguide cross section to the time-averaged energy flow through the entire cross section including the silica cladding [36]. With increasing film thickness, the waveguides exhibit larger mode confinement factors, which means a waveguide with a large cross section can fully confine the mode within the core. For both $n_{2,\mathrm{eff}}$ and Γ, waveguide widths of 1.8 μm and 3 μm have very similar values. Wider 3-μm waveguide widths can support more higher-order modes compared to 1.8-μm waveguide width, which may induce more mode coupling with the fundamental mode and further reduce the Q-factor of the fundamental mode since higher-order modes usually have higher losses [16]. The 1.8-μm waveguide width is already multimode with low loss according to the simulation in Fig. 2(a). Overall, a waveguide with 400-nm height and 1.8-μm waveguide width is optimal for good nonlinear interaction and good mode confinement.
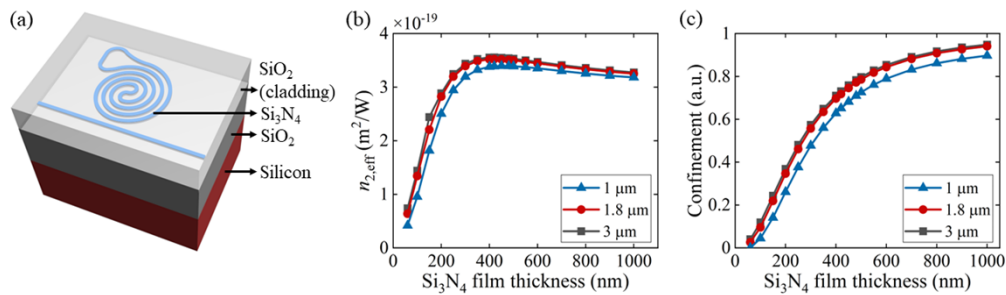
Fig. 1. Design optimization for Si_3N_4 resonators. (a) Schematic view of a Si_3N_4 resonator with silica cladding. Panels (b) and (c) show the simulated effective nonlinear refractive index $n_{2,\mathrm{eff}}$ and mode confinement factor Γ of a Si_3N_4 waveguide as a function of the waveguide thickness for waveguide widths of 1 μm, 1.8 μm, and 3 μm.


Fig. 2. Structure of a compact multimode Si_3N_4 resonator. (a) Mode characterization of the resonator. The bus waveguide has a width of 1 μm and the resonator has a width of 1.8 μm. The resonator supports TE_{00} and TE_{10} modes, which are shown in the simulated mode profiles. (b) Scanning electron microscope image of the resonator.

Based on the 400-nm-thickness Si_3N_4 film, we fabricate Si_3N_4 resonators with 1 μm wide bus waveguides and 1.8 μm resonator widths. The resonator supports both TE_{00} and TE_{10} mode families. Light is injected into the TE_{00} mode (shown in Fig. 2(a)) via the bus waveguide. The shape of the resonator is a spiral [37,38] with a compact footprint of 0.28 mm^2 and an optical path length of 5.9 mm. The gap between the bus waveguide and spiral resonator is 440 nm, which optimizes the coupling efficiency in the L-band wavelength range. For the fabrication of the resonator, we use commercial Si_3N_4 wafers with a 400-nm LPCVD Si_3N_4 layer and a 3 μm silica base layer. The fabrication process starts with spin coating using ma-N 2405 photoresist. Subsequently, the photonic structures are defined with electron-beam lithography, followed by developing and etching. Atomic layer deposition and PECVD are used to form a SiO_2 cladding

with 400 nm and 2.5 μm thickness, respectively. The samples with cladding are then thermally annealed at 1000 °C to break the Si-H and N-H bonds and improve the Q factor. Finally, the bus waveguides are cleaved for edge coupling. The coupling loss is 2 dB/facet. More details of the fabrication can be found in Ref. [39]. Figure 2(b) shows a scanning electron microscope image of the spiral resonator used in this study before adding the SiO_2 cladding.

3. Low-noise dark comb generation

After fabrication, we first characterize the transmission and dispersion of the Si_3N_4 resonator. The experimental setup is shown in Fig. 3(a). A continuous-wave tunable laser is first amplified by an erbium-doped fiber amplifier (EDFA), followed by a polarization controller for matching the polarization with the resonator modes. The light is coupled into and out from the bus waveguide via edge couplers. At the end of the bus waveguide, the light is coupled into three branches: one is monitored by an oscilloscope for recording transmission spectra, the second branch is sent to an optical spectrum analyzer (OSA) for recording comb spectra, and the third branch is sent to a fast photodiode to detect the repetition rate of the generated microcombs and record the corresponding radiofrequency spectra with an electronic spectrum analyzer (ESA). Using low optical power (a few microwatts), the transmission spectrum of the Si_3N_4 resonator was measured and calibrated using a reference fiber cavity from 1550 to 1610 nm [40]. Figure 3(b) shows the transmission spectrum, where two mode families (TE_{00}, and TE_{10}) are excited via the bus waveguide. The marked mode family in Fig. 3(b) is for TE_{00} modes and is used for comb generation. We note that several mode crossings occur at different wavelengths, which assist the dark pulse generation in the normal dispersion regime [15]. In different samples, the
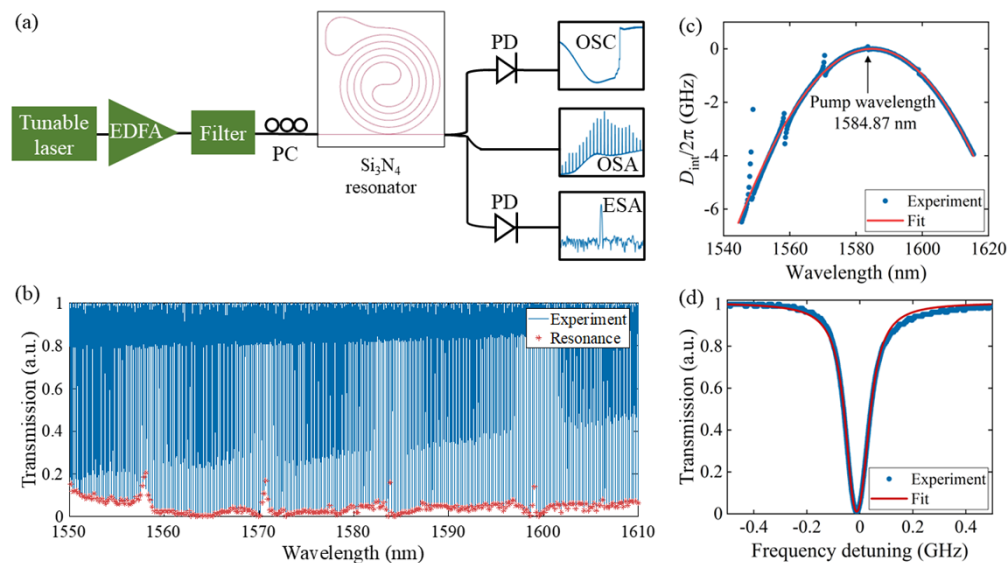
Fig. 3. Transmission and dispersion characterization of the Si_3N_4 resonator. (a) Experimental setup for transmission measurements and dark comb generation. EDFA: erbium-doped fiber amplifier; PC: polarization controller; PD: photodiode; OSC: oscilloscope; OSA: optical spectrum analyzer. ESA: electronic spectrum analyzer. (b) Measured transmission at wavelengths between 1550 nm and 1610 nm. (c) Measured integrated dispersion (D_{int}) for the TE_{00} resonances with a second-order polynomial fit (red solid line). The black arrow marks the pump wavelength of 1584.87 nm for the generation of dark combs. (d) Zoom into a resonance around 1584.87 nm with loaded and intrinsic Q factors of 2×10^6 and 4×10^6, respectively.
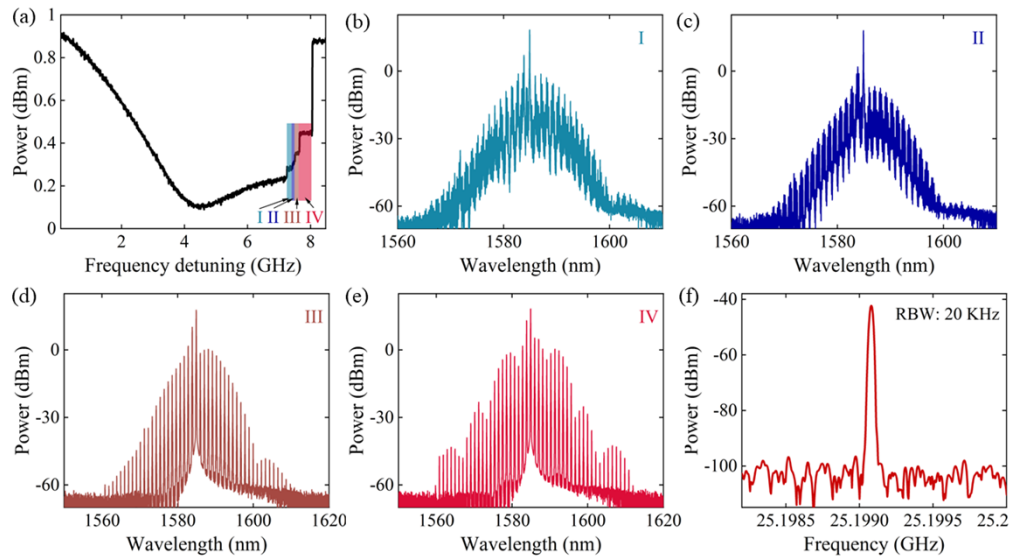
Fig. 4. Measured dark combs in the Si_3N_4 resonator. (a) Normalized transmission of the resonator mode used for comb generation. (b)-(e) Spectra of different dark comb states corresponding to the steps I-IV in (a). (f) Repetition rate beat note corresponding to the comb line spacing of the dark combs around 25 GHz, measured with a resolution bandwidth (RBW) of 20 kHz.

positions of the avoided mode crossings can be slightly different due to the difference in Si_3N_4 thickness from non-uniform wafers and small variations in waveguide widths. In our experiment, we pump a mode at 1584.87 nm to generate low-noise coherent dark pulse combs. The integrated dispersion of this mode family is shown in Fig. 3(c), exhibiting an overall normal dispersion profile while the mode coupling between the TE_{00}-mode family and higher-order mode family at certain wavelengths modifies the local dispersion. Using a second-order polynomial fit, we calculate $D_2/2\pi$ as -380 kHz at this pump wavelength. A zoom into the transmission spectrum around 1584.87 nm and a Lorentzian fit reveals a loaded Q factor of 2×10^6. The intrinsic Q factor is $\sim 4 \times 10^6$, which corresponds to a waveguide loss of 8.5 dB/m. The loaded Q factor of the higher-order mode near the pump wavelength is 4.2×10^5, indicating a higher loss compared to the TE_{00} resonance. In the mode coupling region, the higher-order mode induces a decrease in the Q factor of the TE_{00} resonance due to its higher loss [2].

Next, we investigate the generation of coherent dark combs in the 400-nm-thickness Si_3N_4 resonator. Using the same experimental setup shown in Fig. 3(a), the pump power is increased to excite nonlinear effects in the cavity. Figure 4(a) shows the transmission when pumping a mode at 1584.87 nm with 500 mW on-chip power. Due to thermal and Kerr effects, the resonance transmission has a triangular shape. Most importantly, the transmission has four-step features as marked with I-IV in Fig. 4(a). The measured comb spectra are shown in Fig. 4(b)-(e), corresponding to the different steps in Fig. 4(a). In steps I and II, the spectra of the generated dark comb have a mode spacing of a single FSR. In steps III and IV, the comb spectra have a spacing of five-FSR. This can be explained by the mode crossing that assists the comb generation being five modes away from the pump laser. In the time domain, this pins the dark comb into a state with five dark pulses circulating inside the cavity. We further verify the coherent comb state by measuring the comb line spacing. The comb spectrum is filtered using a tunable fiber Bragg grating filter to suppress the pump power and sent into a fast photodiode. The electronic spectrum of the repetition rate signal is shown in Fig. 4(f) with a resolution bandwidth of 20 kHz.

A single peak around 25 GHz in the RF spectrum is observed with a > 60 dB signal-to-noise ratio, indicating the generated dark comb is in a low-noise and coherent state. We also observe coherent dark comb generation when pumping at laser wavelength near other avoided mode crossings indicated in Fig. 3(c). It should be pointed out that the 400-nm thin Si_3N_4 resonators designed here cannot support bright soliton generation due to normal dispersion. However, the dispersion of thinner Si_3N_4 resonators can be made anomalous via advanced dispersion engineering techniques [41].

4. Conclusion

Optical waveguide dimensions play a critical role in nonlinear optics in microresonators, particularly for Kerr soliton frequency combs. In this work, we have investigated the optical properties of Si_3N_4 resonators with different waveguide thicknesses and widths and applied them to dark soliton generation. Considering factors such as fabrication complexity and nonlinear refractive index, our findings reveal that an optimal compromise between confinement and nonlinearity is achieved with around 400-nm Si_3N_4 films. Si_3N_4 resonators with this thickness and silica cladding can have a maximal nonlinear refractive index of (3.5×10^{-19} m^2/W). Ultra-high quality Si_3N_4 film with a thickness of 400 nm can be deposited in one step without suffering from stress induced cracking. In addition, due to the tight confinement, the requirement for a high-quality SiO_2 layer is mitigated. Based on this analysis, we fabricate 400-nm-thick spiral-shaped Si_3N_4 resonators with a compact footprint of 0.28 mm^2. The resonator exhibits an intrinsic Q factor of 4×10^6. We experimentally demonstrate low-noise dark combs with a repetition rate of 25 GHz. The demonstrated dark soliton combs can be useful for precision spectroscopy [40,42], on-chip light detection and ranging (LIDAR) [43,44], microwave photonics [45–52] including RF transversal filters [46] and differentiators [53], as well as in telecommunication systems [54], optical computing [55] and quantum optics [56].

Disclosures. The authors declare that they have no conflicts of interest.

Data availability. The data used in this study are available from the corresponding authors upon reasonable request.

References

1. Z. Ye, H. Jia, Z. Huang, C. Shen, J. Long, B. Shi, Y.-H. Luo, L. Gao, W. Sun, and H. Guo, "Foundry manufacturing of tight-confinement, dispersion-engineered, ultralow-loss silicon nitride photonic integrated circuits," Photonics Res. **11**(4), 558–568 (2023).
2. Y. Zhang, K. Zhong, X. Zhou, and H. K. Tsang, "Broadband high-Q multimode silicon concentric racetrack resonators for widely tunable Raman lasers," Nat. Commun. **13**(1), 3534 (2022).
3. Y. Zhang, K. Zhong, and H. K. Tsang, "Raman lasing in multimode silicon racetrack resonators," Laser Photonics Rev. **15**(2), 2000336 (2021).
4. A. Dutt, C. Joshi, X. Ji, J. Cardenas, Y. Okawachi, K. Luke, A. L. Gaeta, and M. Lipson, "On-chip dual-comb source for spectroscopy," Sci. Adv. **4**(3), e1701858 (2018).
5. P. J. Marchand, J. Riemensberger, J. C. Skehan, J.-J. Ho, M. H. Pfeiffer, J. Liu, C. Hauger, T. Lasser, and T. J. Kippenberg, "Soliton microcomb based spectral domain optical coherence tomography," Nat. Commun. **12**(1), 427 (2021).
6. M. Siddiqui, A. S. Nam, S. Tozburun, N. Lippok, C. Blatter, and B. J. Vakoc, "High-speed optical coherence tomography by circular interferometric ranging," Nat. Photonics **12**(2), 111–116 (2018).
7. P. Marin-Palomo, J. N. Kemal, M. Karpov, A. Kordts, J. Pfeifle, M. H. Pfeiffer, P. Trocha, S. Wolf, V. Brasch, and M. H. Anderson, "Microresonator-based solitons for massively parallel coherent optical communications," Nature **546**(7657), 274–279 (2017).
8. K. Y. Yang, C. Shirpurkar, A. D. White, J. Zang, L. Chang, F. Ashtiani, M. A. Guidry, D. M. Lukin, S. V. Pericherla, and J. Yang, "Multi-dimensional data transmission using inverse-designed silicon photonics and microcombs," Nat. Commun. **13**(1), 7862 (2022).

9. C. Xiang, J. Liu, J. Guo, L. Chang, R. N. Wang, W. Weng, J. Peters, W. Xie, Z. Zhang, and J. Riemensberger, "Laser soliton microcombs heterogeneously integrated on silicon," Science **373**(6550), 99–103 (2021).

10. H. Shu, L. Chang, Y. Tao, B. Shen, W. Xie, M. Jin, A. Netherton, Z. Tao, X. Zhang, and R. Chen, "Microcomb-driven silicon photonic systems," Nature **605**(7910), 457–463 (2022).

11. J. Feldmann, N. Youngblood, M. Karpov, H. Gehring, X. Li, M. Stappers, M. Le Gallo, X. Fu, A. Lukashchuk, and A. S. Raja, "Parallel convolutional processing using an integrated photonic tensor core," Nature **589**(7840), 52–58 (2021).

12. T. Herr, V. Brasch, J. D. Jost, C. Y. Wang, N. M. Kondratiev, M. L. Gorodetsky, and T. J. Kippenberg, "Temporal solitons in optical microresonators," Nat. Photonics **8**(2), 145–152 (2014).

13. F. Lei, Z. Ye, Ó. B. Helgason, A. Fülöp, M. Girardi, and V. Torres-Company, "Optical linewidth of soliton microcombs," Nat. Commun. **13**(1), 3161 (2022).

14. X. Ji, J. Liu, J. He, R. N. Wang, Z. Qiu, J. Riemensberger, and T. J. Kippenberg, "Compact, spatial-mode-interaction-free, ultralow-loss, nonlinear photonic integrated circuits," Commun. Phys. **5**(1), 84 (2022).

15. X. Xue, Y. Xuan, Y. Liu, P.-H. Wang, S. Chen, J. Wang, D. E. Leaird, M. Qi, and A. M. Weiner, "Mode-locked dark pulse Kerr combs in normal-dispersion microresonators," Nat. Photonics **9**(9), 594–600 (2015).

16. S. Kim, K. Han, C. Wang, J. A. Jaramillo-Villegas, X. Xue, C. Bao, Y. Xuan, D. E. Leaird, A. M. Weiner, and M. Qi, "Dispersion engineering and frequency comb generation in thin silicon nitride concentric microresonators," Nat. Commun. **8**(1), 372 (2017).

17. S. Zhang, T. Bi, G. N. Ghalanos, N. P. Moroney, L. Del Bino, and P. Del'Haye, "Dark-bright soliton bound states in a microresonator," Phys. Rev. Lett. **128**(3), 033901 (2022).

18. M. H. Anderson, W. Weng, G. Lihachev, A. Tikan, J. Liu, and T. J. Kippenberg, "Zero dispersion Kerr solitons in optical microresonators," Nat. Commun. **13**(1), 4764 (2022).

19. S. Zhang, T. Bi, and P. Del'Haye, "Quintic dispersion soliton frequency combs in a microresonator," Laser Photonics Rev. **17**(10), 2300075 (2023).

20. Q.-X. Ji, W. Jin, L. Wu, Y. Yu, Z. Yuan, W. Zhang, M. Gao, B. Li, H. Wang, and C. Xiang, "Engineered zero-dispersion microcombs using CMOS-ready photonics," Optica **10**(2), 279–285 (2023).

21. Z. Xiao, T. Li, M. Cai, H. Zhang, Y. Huang, C. Li, B. Yao, K. Wu, and J. Chen, "Near-zero-dispersion soliton and broadband modulational instability Kerr microcombs in anomalous dispersion," Light: Sci. Appl. **12**(1), 33 (2023).

22. J. Liu, G. Huang, R. N. Wang, J. He, A. S. Raja, T. Liu, N. J. Engelsen, and T. J. Kippenberg, "High-yield, wafer-scale fabrication of ultralow-loss, dispersion-engineered silicon nitride photonic circuits," Nat. Commun. **12**(1), 2236 (2021).

23. K. J. McNulty, X. Ji, A. Gil-Molina, M. Corato-Zanarella, G. R. Bhatt, I. Datta, S. Chaitanya, Y. Okawachi, A. L. Gaeta, and M. Lipson, "Low stress bilayer LPCVD-PECVD SiN waveguides for Kerr frequency comb generation," in *CLEO: Science and Innovations* (Optica Publishing Group, 2023), STh1J.2.

24. K. Wu and A. W. Poon, "Stress-released Si_3N_4 fabrication process for dispersion-engineered integrated silicon photonics," Opt. Express **28**(12), 17708–17722 (2020).

25. V. Lobanov, G. Lihachev, T. Kippenberg, and M. Gorodetsky, "Frequency combs and platicons in optical microresonators with normal GVD," Opt. Express **23**(6), 7713–7721 (2015).

26. Y. Liu, Y. Xuan, X. Xue, P.-H. Wang, S. Chen, A. J. Metcalf, J. Wang, D. E. Leaird, M. Qi, and A. M. Weiner, "Investigation of mode coupling in normal-dispersion silicon nitride microresonators for Kerr frequency comb generation," Optica **1**(3), 137–144 (2014).

27. X. Xue, P. H. Wang, Y. Xuan, M. Qi, and A. M. Weiner, "Microresonator Kerr frequency combs with high conversion efficiency," Laser Photonics Rev. **11**(1), 1600276 (2017).

28. X. Xue, Y. Xuan, P. H. Wang, Y. Liu, D. E. Leaird, M. Qi, and A. M. Weiner, "Normal-dispersion microcombs enabled by controllable mode interactions," Laser Photonics Rev. **9**, L23–L28 (2015).

29. Y. Xuan, Y. Liu, L. T. Varghese, A. J. Metcalf, X. Xue, P.-H. Wang, K. Han, J. A. Jaramillo-Villegas, A. Al Noman, and C. Wang, "High-Q silicon nitride microresonators exhibiting low-power frequency comb initiation," Optica **3**(11), 1171–1180 (2016).

30. A. Fülöp, M. Mazur, A. Lorences-Riesgo, Ó. B. Helgason, P.-H. Wang, Y. Xuan, D. E. Leaird, M. Qi, P. A. Andrekson, and A. M. Weiner, "High-order coherent communications using mode-locked dark-pulse Kerr combs from microresonators," Nat. Commun. **9**(1), 1598 (2018).

31. A. Jørgensen, D. Kong, M. Henriksen, F. Klejs, Z. Ye, O. Helgason, H. Hansen, H. Hu, M. Yankov, and S. Forchhammer, "Petabit-per-second data transmission using a chip-scale microcomb ring resonator source," Nat. Photonics **16**(11), 5 (2022).

32. Z. Ye, K. Twayana, and P. A. Andrekson, "High-Q Si_3N_4 microresonators based on a subtractive processing for Kerr nonlinear optics," Opt. Express **27**(24), 35719–35727 (2019).

33. W. Jin, Q.-F. Yang, L. Chang, B. Shen, H. Wang, M. A. Leal, L. Wu, M. Gao, A. Feshali, and M. Paniccia, "Hertz-linewidth semiconductor lasers using CMOS-ready ultra-high-Q microresonators," Nat. Photonics **15**(5), 346–353 (2021).

34. B. Shen, L. Chang, J. Liu, H. Wang, Q.-F. Yang, C. Xiang, R. N. Wang, J. He, T. Liu, and W. Xie, "Integrated turnkey soliton microcombs," Nature **582**(7812), 365–369 (2020).

35. S. Afshar and T. M. Monro, "A full vectorial model for pulse propagation in emerging waveguides with subwavelength structures part I: Kerr nonlinearity," Opt. Express **17**(4), 2298–2318 (2009).

36. P. Steglich and K. You, "Silicon-on-insulator slot waveguides: theory and applications in electro-optics and optical sensing," in *Emerging Waveguide Technology* (2018), pp. 187–210.

37. T. Chen, H. Lee, J. Li, and K. J. Vahala, "A general design algorithm for low optical loss adiabatic connections in waveguides," Opt. Express **20**(20), 22819–22829 (2012).

38. Z. Ye, F. Lei, K. Twayana, M. Girardi, P. A. Andrekson, and V. Torres-Company, "Integrated, ultra-compact high-Q silicon nitride microresonators for low-repetition-rate soliton microcombs," Laser Photonics Rev. **16**(3), 2100147 (2022).

39. S. Zhang, T. Bi, I. Harder, O. Lohse, F. Gannott, A. Gumann, Y. Zhang, and P. Del'Haye, "Room-temperature sputtered ultralow-loss silicon nitride for hybrid photonic integration," arXiv, arXiv:2301.10758 (2023).

40. S. Zhang, T. Bi, and P. Del'Haye, "On-the-fly precision spectroscopy with a dual-modulated tunable diode laser and Hz-level referencing to a cavity," arXiv, arXiv:2303.14180 (2023).

41. Z. Yuan, M. Gao, Y. Yu, H. Wang, W. Jin, Q.-X. Ji, A. Feshali, M. Paniccia, J. Bowers, and K. Vahala, "Soliton pulse pairs at multiple colors in normal dispersion microresonators," Nat. Photon. **1**, 1 (2023).

42. P. Del'Haye, O. Arcizet, M. L. Gorodetsky, R. Holzwarth, and T. J. Kippenberg, "Frequency comb assisted diode laser spectroscopy for measurement of microcavity dispersion," Nat. Photonics **3**(9), 529–533 (2009).

43. N. Kuse and M. E. Fermann, "Frequency-modulated comb LIDAR," APL Photonics **4**(10), 106105 (2019).

44. R. Chen, H. Shu, B. Shen, L. Chang, W. Xie, W. Liao, Z. Tao, J. E. Bowers, and X. Wang, "Breaking the temporal and frequency congestion of LiDAR by parallel chaos," Nat. Photonics **17**(4), 306–314 (2023).

45. J. Liu, E. Lucas, A. S. Raja, J. He, J. Riemensberger, R. N. Wang, M. Karpov, H. Guo, R. Bouchand, and T. J. Kippenberg, "Photonic microwave generation in the X-and K-band using integrated soliton microcombs," Nat. Photonics **14**(8), 486–491 (2020).

46. M. Tan, X. Xu, J. Wu, R. Morandotti, and D. Moss, "Ultra-high bandwidth radio frequency and microwave photonic signal processing based on kerr micro-combs," Adv. Phys.: X **6**(1), 1838946 (2021).

47. Q.-F. Yang, Q.-X. Ji, L. Wu, B. Shen, H. Wang, C. Bao, Z. Yuan, and K. Vahala, "Dispersive-wave induced noise limits in miniature soliton microwave sources," Nat. Commun. **12**(1), 1442 (2021).

48. E. A. Kittlaus, D. Eliyahu, S. Ganji, S. Williams, A. B. Matsko, K. B. Cooper, and S. Forouhar, "A low-noise photonic heterodyne synthesizer and its application to millimeter-wave radar," Nat. Commun. **12**(1), 4397 (2021).

49. M. H. Anderson, R. Bouchand, J. Liu, W. Weng, E. Obrzud, T. Herr, and T. J. Kippenberg, "Photonic chip-based resonant supercontinuum via pulse-driven Kerr microresonator solitons," Optica **8**(6), 771–779 (2021).

50. T. M. Fortier, M. S. Kirchner, F. Quinlan, J. Taylor, J. Bergquist, T. Rosenband, N. Lemke, A. Ludlow, Y. Jiang, and C. Oates, "Generation of ultrastable microwaves via optical frequency division," Nat. Photonics **5**(7), 425–429 (2011).

51. Y. Sun, J. Wu, M. Tan, X. Xu, Y. Li, R. Morandotti, A. Mitchell, and D. J. Moss, "Applications of optical microcombs," Adv. Opt. Photonics **15**(1), 86–175 (2023).

52. J. Wu, X. Xu, T. G. Nguyen, S. T. Chu, B. E. Little, R. Morandotti, A. Mitchell, and D. J. Moss, "RF photonics: an optical microcombs' perspective," IEEE J. Sel. Top. Quantum Electron. **24**(4), 1–20 (2018).

53. X. Xu, J. Wu, M. Shoeiby, T. G. Nguyen, S. T. Chu, B. E. Little, R. Morandotti, A. Mitchell, and D. J. Moss, "Reconfigurable broadband microwave photonic intensity differentiator based on an integrated optical frequency comb source," APL Photonics **2**(9), 096104 (2017).

54. Y. Geng, H. Zhou, X. Han, W. Cui, Q. Zhang, B. Liu, G. Deng, Q. Zhou, and K. Qiu, "Coherent optical communications using coherence-cloned Kerr soliton microcombs," Nat. Commun. **13**(1), 1070 (2022).

55. X. Xu, M. Tan, B. Corcoran, J. Wu, A. Boes, T. G. Nguyen, S. T. Chu, B. E. Little, D. G. Hicks, R. Morandotti, A. Mitchell, and D. J. Moss, "11 TOPS photonic convolutional accelerator for optical neural networks," Nature **589**(7840), 44–51 (2021).

56. M. Kues, C. Reimer, J. M. Lukens, W. J. Munro, A. M. Weiner, D. J. Moss, and R. Morandotti, "Quantum optical microcombs," Nat. Photonics **13**(3), 170–179 (2019).